

Analysis of the thin layer of Galactic warm ionized gas in the range $20^\circ < l < 30^\circ$, $-1.5^\circ < b < +1.5^\circ$

R. Paladini^{1*}, G. De Zotti^{2†}, R. D. Davies^{3‡}, M. Giard^{1§}

¹ *CESR, 9, Avenue du Colonel Roche, Boite postale 4346, F-31028 Toulouse, France*

² *INAF-Osservatorio Astronomico di Padova, Vicolo dell'Osservatorio 5, I-35122 Padova, Italy*

³ *University of Manchester, Jodrell Bank Observatory, Macclesfield - Cheshire SK11 9DL, UK*

12 June 2018

ABSTRACT

We present an analysis of the thin layer of Galactic warm ionized gas at an angular resolution $\sim 10'$. This is carried out using radio continuum data at 1.4 GHz, 2.7 GHz and 5 GHz in the coordinate region $20^\circ < l < 30^\circ$, $-1.5^\circ < b < +1.5^\circ$. For this purpose, we evaluate the zero level of the 2.7 and 5 GHz surveys using auxiliary data at 2.3 GHz and 408 MHz. The derived zero level corrections are $T_{\text{zero}}(2.7 \text{ GHz}) = 0.15 \pm 0.06 \text{ K}$ and $T_{\text{zero}}(5 \text{ GHz}) = 0.1 \pm 0.05 \text{ K}$. We separate the thermal (free-free) and non-thermal (synchrotron) component by means of a spectral analysis performed adopting an antenna temperature spectral index -2.1 for the free-free emission, a realistic spatial distribution of indices for the synchrotron radiation and by fitting, pixel-by-pixel, the Galactic spectral index. We find that at 5 GHz, for $|b| = 0^\circ$, the fraction of thermal emission reaches a maximum value of 82%, while at 1.4 GHz, the corresponding value is 68%. In addition, for the thermal emission, the analysis indicates a dominant contribution of the diffuse component relative to the source component associated with discrete HII regions.

Key words: Warm ionized gas – Galaxy: structure – radio continuum: ISM

1 INTRODUCTION

The spatial distribution of the Galactic Warm Ionized Medium (WIM) is characterized by a thin and a thick layer. The *thin layer* consists of ionized gas located on the Galactic plane and composed of discrete HII regions and diffuse gas. The *thick layer* consists instead of the ionized gas which is situated well above the plane and presents only a diffuse-gas component. Current models of the WIM (Miller & Cox 1993; Domgörgen & Mathis 1994) tend to favour a scenario in which the presence of ionized gas in the thick layer is due to ultraviolet radiation leaking out of regions of star formation located in the thin layer. In the light of these models, knowledge of the physical properties of the thin layer is crucial for understanding the mechanisms regulating the global distribution of the warm ionized gas. However, despite its relevance, systematic investigations of the thin layer have not been carried out to date. Complementary information on the WIM comes from pulsar dispersion measurements (DMs) which are linearly weighted by the electron density,

n_e , rather than weighted by n_e^2 as in the case of the $H\alpha$ and of the radio free-free emission discussed here. The DM data imply an inner Galactic electron layer of scale height $\sim 150 \text{ pc}$ (Taylor & Cordes 1993); these data are spatially undersampled however and do not have the angular resolution of the data used in the present study.

This paper investigates the thin layer by combining the information on the diffuse component derived from radio continuum surveys with the information on the Galactic HII region distribution as given in Paladini, Davies & De Zotti (2003). In particular, we estimate the contribution of the discrete, HII component with respect to the diffuse component. We emphasize that our analysis is also of interest for foreground studies in the context of CMB observations as well as for investigations of the ISM. The paper is organized as follows. In Sect. 2 we present the data base used for the analysis. In Sect. 3 we discuss the importance of an accurate determination of the zero levels for the surveys involved and we describe the methods applied to our case. In Sect. 4 we illustrate the results of the component separation technique in deriving the latitude distribution of free-free and synchrotron emission. In Sect. 5 we estimate the contribution of discrete HII regions to the total free-free emissions.

* E-mail: paladini@cesr.fr

† E-mail: dezotti@pd.astro.it

‡ E-mail: rdd@jb.man.ac.uk

§ E-mail: giard@cesr.fr

2 CHOICE OF THE DATA BASE

For the analysis of the diffuse ionized gas adjacent to the Galactic plane, we make use of radio continuum data. As well known, an ionized gas in the physical conditions of the interstellar medium ($T_e \sim 10^4$ K, $n_e \sim 0.1 \text{ cm}^{-3}$) emits a continuum spectrum at radio frequencies due to Coulomb interaction of free electrons with ions (thermal bremsstrahlung or *free-free radiation*). The use of radio data offers various advantages with respect to other tracers: this continuum radiation is not subject to extinction from interstellar dust grains (as the $H\alpha$ emission) and it does not suffer from undersampling (as in the case of pulsar dispersion measures). An important drawback, however, for radio continuum data results from the fact that the observed emission is the superposition of the free-free emission and of the synchrotron radiation produced by relativistic electrons accelerated in the Galactic magnetic field. Therefore, the use of such data for investigating the ionized gas requires a decomposition of the observed signal into its constituents. This can be achieved by exploiting the spectral dependence of each component when data are available at least at two frequencies.

The first step is the selection of a region of the Galaxy in which to carry out the analysis. This is followed by the choice of the data sets covering the selected region. For the selection of the Galactic region we follow these guidelines: we look for an area surveyed at several frequencies, close to the plane and in a longitude range where we expect the emission from the ionized gas to be particularly bright. At the same time, we try to avoid regions in which the source of emission is not fully understood such as areas located in the proximity of the Galactic centre. According to these criteria, we select the longitude range $20^\circ < l < 30^\circ$ which includes the Sagittarius-Carina and the Scutum-Crux arms; the latter is tangent at $l \sim 30^\circ$. The Galactic plane emission is well-defined in this region.

The three surveys with accurate calibrations and well-determined baselines are the 1.4 GHz survey by Reich et al. (1990a), the 2.7 GHz survey by Reich et al. (1990b) and the 5 GHz survey by Haynes et al. (1978). They cover a sufficient frequency range for an adequate separation of synchrotron and free-free emission components. It is also important to stress that the angular resolution of these surveys enables us to perform an analysis of the warm ionized gas in the Galactic plane on a $10'$ scale. It is for this reason that we have not used the 408 MHz data of Haslam et al. (1982) at $51'$ resolution. Our study, as a consequence, covers the latitude range $-1.5^\circ < b < 1.5^\circ$ defined by the 5 GHz survey.

All the maps used for this work have been downloaded from the MPIFR web site: <http://www.mpifr-bonn.mpg.de/survey.html>. Details about the surveys are given below and summarized in Table 1.

2.1 The 1.4 GHz survey

The 1.4 GHz data are derived from a continuum survey of the Galactic plane carried out with the Effelsberg 100-m telescope at an angular resolution of $9.35'$ in the coordinate range $-3^\circ < l < 240^\circ$, $-4^\circ < b < 4^\circ$. The baseline level of the total intensity map has been determined from the large area Stockert 1.4 GHz survey (Reich 1982; Reich & Reich

Table 1. Summary of the surveys

<i>Survey</i>	ν	HPBW	Sky coverage
Effelsberg 100-m	1.4 GHz	9.4'	$-3^\circ < l < 240^\circ$ $-4^\circ < b < 4^\circ$
Effelsberg 100-m	2.7 GHz	4.3'	$-2^\circ < l < 240^\circ$ $-5^\circ < b < 5^\circ$
Parkes 64-m	5 GHz	4.1'	$-170^\circ \leq l \leq 40^\circ$ $-1.5^\circ \leq b \leq 1.5^\circ$

1986) made with a resolution of $35.9'$. The absolute level of emission is derived by comparison with the Howell & Shakeshaft (1967) measurements and is believed to be accurate to 0.5 K. The temperature calibration based on standard radio sources is accurate to $\pm 5\%$. The Reich et al. (1990a) survey, corrected for the CMB and unresolved extragalactic sources (see Section 3) is adopted as the reference survey for the present analysis. It is plotted in Fig. 1.

2.2 The 2.7 GHz survey

The 2.7 GHz data have been obtained with the Effelsberg 100-m telescope. The survey is characterized by an angular resolution of $4.3'$ and covers the coordinate range $-2^\circ < l < 240^\circ$, $-5^\circ < b < 5^\circ$. The latitude range $-1.5^\circ < b < 1.5^\circ$ was scanned in Galactic latitude with a scan separation of $2'$. The latitude range $|b| = 1.5^\circ$ to 4° was scanned at the same scan separation but in both Galactic coordinates. For $-2^\circ < l < 76^\circ$ the large-scale structures have been added by using low-resolution data ($\sim 19'$) at 2.7 GHz taken with the Stockert telescope (Reif et al. 1987). Zero level fluctuations are reported of order of 100 mK. The Effelsberg data and the low-resolution data have been combined into a final map. The temperature calibration accuracy is believed to be $\pm 5\%$. The 2.7 GHz data corrected for the CMB and extragalactic sources are plotted in Fig. 1.

2.3 The 5 GHz survey

The 5 GHz survey was made using the Parkes 64-m telescope and has an angular resolution of $4.1'$. It covers $-170^\circ \leq l \leq 40^\circ$ and $-1.5^\circ \leq b \leq +1.5^\circ$. The primary scan direction was chosen to be either right ascension or declination, whichever was nearer to being orthogonal to the Galactic plane. In particular, the longitude range $20^\circ \leq l \leq 30^\circ$ was scanned in right ascension, with primary scans separated by $2'$. The region of the sky to be surveyed was divided into blocks, each block being ~ 16 square degrees in area. Baseline levels within each block were set by reference to two tie-down scans to points well off the Galactic plane so as to determine a consistent base level. The baseline uncertainty was estimated to be 0.2 K and the temperature accuracy was $\pm 10\%$.

A few steps of data processing have been taken prior to the realization of the component separation. The 5 GHz map is characterized by a significant number of negative pixels – typically at the border of the map – which correspond to unobserved regions and result from the adopted scanning

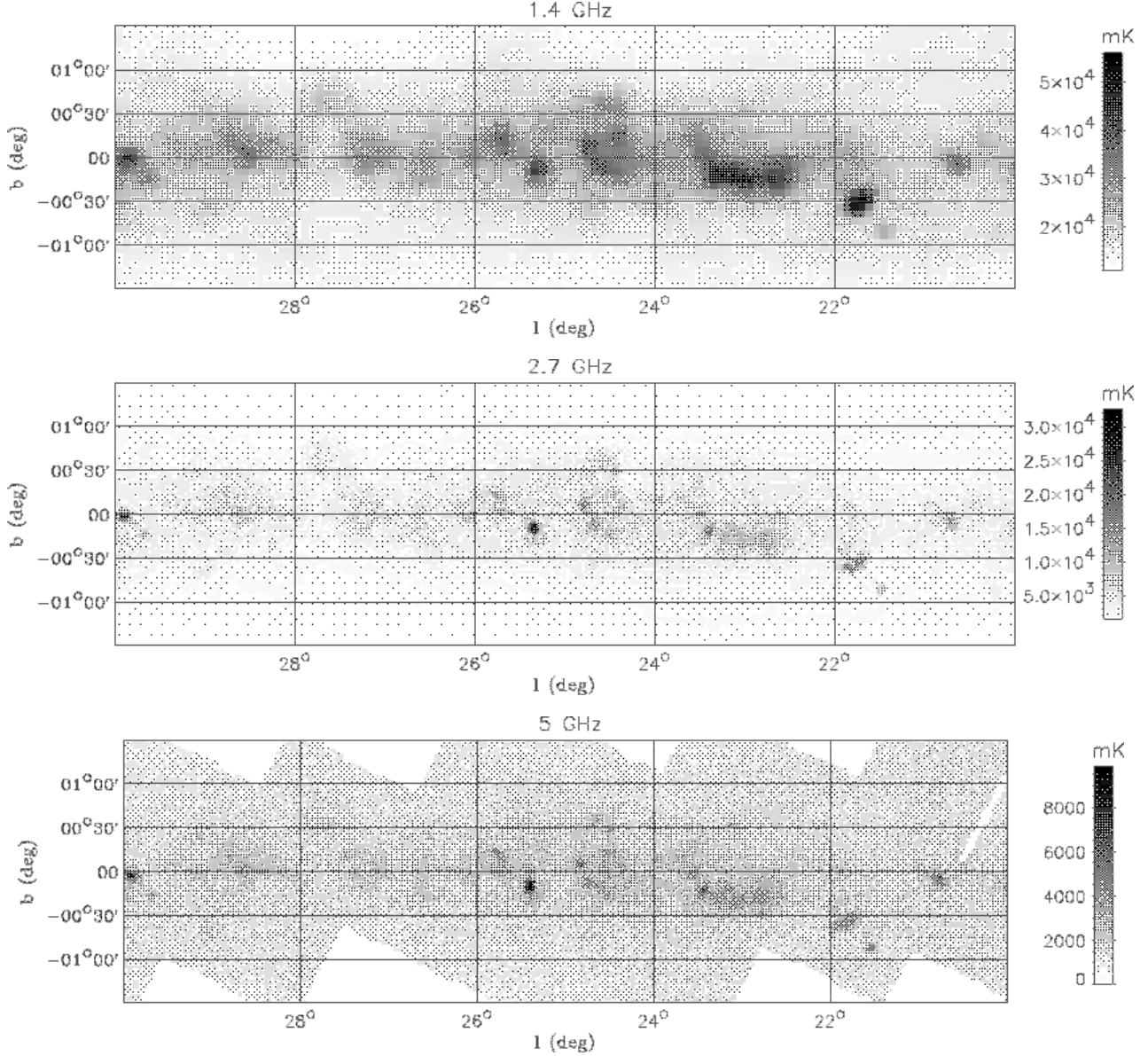


Figure 1. The selected Galactic region $20^\circ < l < 30^\circ$ and $-1.5^\circ < b < +1.5^\circ$ in the 1.4 GHz survey (top panel), 2.7 GHz survey (central panel) and 5 GHz survey (bottom panel). The background due to the CMB and extragalactic sources has been removed.

strategy. No interpolation over these bad pixels has been performed since these regions are far too extended to allow us to fill the gaps in a realistic, reliable way. We have therefore carried out our analysis considering, for each frequency, only the pixels with a positive, detected signal. All the maps have been pixelized at the level of the 5 GHz map, i.e. to $2'$ pixel and the 2.7 and 5 GHz maps have been convolved to $9.4'$, the angular resolution of the 1.4 GHz map. Due to the missing pixel problem, the convolution introduces some level of error in the 5 GHz map. However, this error concerns only a very limited number of pixels (namely, the ones at the scan borders) and we expect it not to be dominant in the global error budget.

3 ZERO LEVEL DETERMINATION

As mentioned in the introduction, it is possible to perform the separation of the free-free emission from the synchrotron emission by exploiting the information on their spectral behaviour. However, this method is subject to large errors if the zero levels of each survey have not been accurately determined. Following Reich & Reich (1988), we write the observed sky brightness temperature T at any point and at a frequency ν as the sum of various contributions:

$$T(\nu) = T_{\text{gal}}(\nu) + T_{\text{cmb}} + T_{\text{ex}}(\nu) + T_{\text{zero}}(\nu). \quad (1)$$

In Eq. (1), $T_{\text{gal}}(\nu)$ is the Galactic brightness temperature; T_{cmb} is the brightness temperature of the Cosmic Microwave Background ($T_{\text{cmb}} = 2.728 \pm 0.004$ K, Fixsen et al. 1996); $T_{\text{ex}}(\nu)$ is the contribution of the unresolved extragalactic sources; $T_{\text{zero}}(\nu)$ is the zero level correction. The contribu-

tion of the extragalactic background is of order of few mK at these frequencies, i.e. much less than any baseline uncertainty, so that it can be neglected in the calculation.

While the zero level of the 1.4 GHz survey has been accurately set, the zero levels of the 2.7 and 5 GHz surveys have to be estimated. For this purpose, we make use of auxiliary data at 408 MHz (Haslam et al. 1982) and 2.3 GHz (Jonas et al. 1998). The Haslam full-sky survey has an angular resolution of 0.85° and its temperature scale is believed to be accurate to within 10%. In addition, it is characterized by a well-known offset of 3 K. We have used the version of the 408-MHz survey obtained by D.P. Finkbeiner, M. Davis & D. Schlegel (private communication). They have removed point sources and destriped the map by applying a Fourier filtering technique. The 2.3 GHz survey, which has been carried out with the HartRAO 26-m telescope, covers 67% of the sky with a resolution of $20'$. The estimated uncertainty in the temperature scale is less than 5% and the quoted error in the absolute zero is 80 mK in any direction. The version of the 2.3 GHz map that we have used is that supplied by Platanina et al. (2003) which has point sources removed and has been destriped. It is important to point out that the Jonas et al. survey is polarization dependent and its absolute zero level has been set by comparison with the Haslam et al. 408 MHz survey. This fact implies that our determination of the 2.7 and 5 GHz zero levels are based both, in practice, on the 408 MHz baseline accuracy. At each frequency (2.7 and 5 GHz), the strategy adopted for setting the zero level takes into account the specific features of the survey. The Effelsberg 11-com survey extends up to $b = \pm 5^\circ$. For these latitudes, in the region $20^\circ < l < 30^\circ$, we estimate the contribution from the free-free emission. This is obtained using the Dickinson et al. (2003) $H\alpha$ map. Following the lines described in the paper, the observed $H\alpha$ is first corrected for absorption by means of the $100\text{-}\mu\text{m}$ dust template given by Schlegel, Finkbeiner & Davis (1998) and the assumption of a non-uniform mixing of ionized gas and dust¹. The corrected $H\alpha$ is then converted into free-free emission using Eq. (11) in the Dickinson et al. paper. The derived free-free emission contribution is shown in Fig. 2.

As stated in Sect. 2, the $H\alpha$ is not a reliable indicator of free-free emission for regions close to the Galactic plane. However, as the figure shows, at $b = \pm 5^\circ$ the derived free-free emission still agrees with a cosecant law while for $|b| < 5^\circ$ and, in particular, $|b| < 3\text{--}4^\circ$, a clear departure sets in. Up to $b = \pm 5^\circ$, the free-free emission contribution at 2.3 GHz is negligible with respect to the total emission which, consequently, is dominated by synchrotron radiation. We make use of the Giardino et al. (2002) spectral index map to extrapolate the 2.3 GHz data to 2.7 GHz. Details on the Giardino et al. map will be given in Sect. 4.1. Here we only emphasize that, although this is generally known to be a pure synchrotron spectral index map, no actual decomposition of the thermal and non-thermal emission has been performed in the original data. However, we have shown that up to ~ 2 GHz, the observed emission is basically synchrotron radiation for $|b| > 3\text{--}4^\circ$. After convolving the

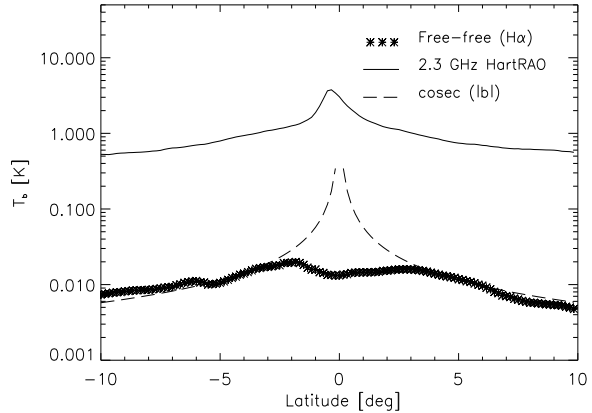


Figure 2. Free-free emission contribution (crosses) at 2.3 GHz (observed emission denoted with a solid line) estimated from the Dickinson et al. (2003) $H\alpha$ map. The profiles have been obtained by averaging over $10'$ slices in latitude from $l = 20^\circ$ to 30° . Shown in the figure (dashed line), for comparison, is also the best-fitting cosecant law for the free-free emission distribution. Note the logarithmic scale on the vertical axis.

2.7 GHz data at the 2.3 GHz resolution, a latitude profile extending out to $b = \pm 5^\circ$ is obtained by averaging the total brightness temperature, corrected for the CMB, over the longitude range 20° to 30° . The zero level at 2.7 GHz is estimated at $b = \pm 5^\circ$ by extrapolating the 2.3 GHz data in frequency (see Fig. 3, top panel). The best estimate of $T_{\text{zero}}(2.7 \text{ GHz}) = 0.15 \pm 0.06 \text{ K}$ which is slightly larger than the zero level uncertainty of 0.1 K given by Reich et al. (1990b).

The estimate of the zero level for the Parkes 6-cm survey is more complicated. The observed region does not extend beyond $|b| = 1.5^\circ$. At these low latitudes, the $H\alpha$ cannot be used to trace the free-free emission. Moreover, the thermal fraction is expected to represent a significant part of the emission. We then proceed along these lines. We first notice that, as reported by Broadbent et al. (1989), the digitized version of the map has a constant offset added of 1 K. We subtract this offset from the data. We then consider the region $l = 5^\circ$ to 10° , $|b| \leq 1.5^\circ$ in which the number of bad (=empty) pixels is negligible, even at the scan borders. As reported by Haynes et al. (1978), out of 150 blocks in which the whole surveyed area has been divided, only 3 show baseline discrepancies and, in this case, a baseline adjustment to bring these blocks into line has been performed. This means that we can evaluate the absolute zero level in the region $5^\circ < l < 10^\circ$ and confidently adopt such an estimate in the region $20^\circ < l < 30^\circ$. For $l = 5^\circ$ to 10° , $|b| \leq 1.5^\circ$, we fit the spectral indices between 408 MHz and 2.3 GHz. We use these spectral indices to extrapolate the 2.3 GHz data to 5 GHz. This operation may formally introduce an error. However, given the fact that we extrapolate out of the fitting interval but to a nearby frequency, we can assume such an error to be small. The 5 GHz data, convolved to the larger 2.3 GHz beam, are used to derive a latitude profile extending up to $b = \pm 1.5^\circ$. The zero level is obtained by comparison, at $|b| = 1.5^\circ$, with the expected profile from the extrapolated 2.3 GHz data (Fig. 3, bottom panel). The

¹ In their paper, Dickinson et al. define f_d as the effective dust fraction in the line of sight actually absorbing the $H\alpha$ and set $f_d = 0.33$.

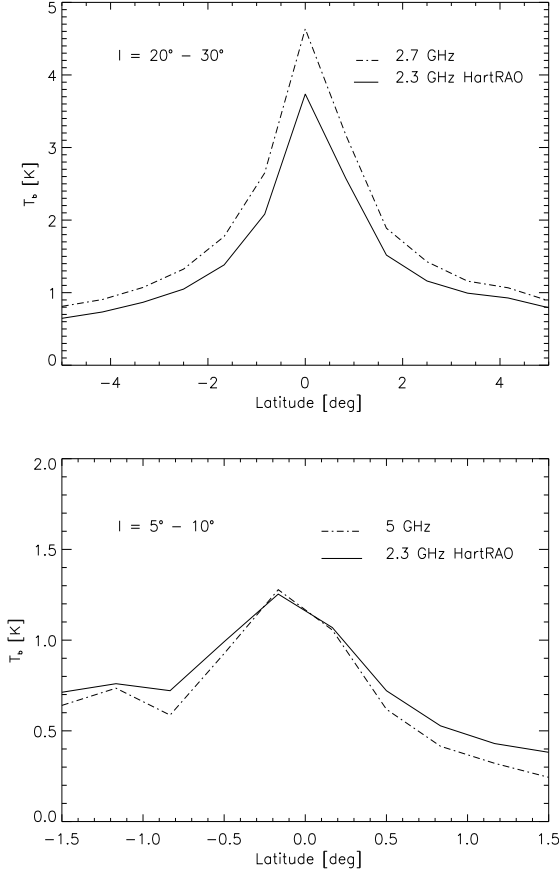


Figure 3. The dashed lines show the latitude profiles for the 2.7 GHz survey (top panel) and for the 5 GHz survey (bottom panel). The solid lines denote the 2.3 GHz data scaled to the relevant frequency (2.7 or 5 GHz). Profiles have been obtained by averaging over $20'$ slices in latitude from $l = 20^\circ$ to 30° at 2.7 GHz and from $l = 5^\circ$ to 10° at 5 GHz.

best estimate, $T_{\text{zero}}(5 \text{ GHz}) = 0.10 \pm 0.05 \text{ K}$, is comparable to the uncertainty of 0.2 K quoted by Haynes et al. (1978).

4 SPECTRAL ANALYSIS AND COMPONENT SEPARATION

Having set and removed the zero levels at each considered frequency, we can perform the component separation. At a given frequency ν , the brightness temperature $T_{\text{gal}}(\nu)$ of a single pixel can be written as:

$$T_{\text{gal}}(\nu) = T_{\text{ff}}(\nu) + T_{\text{syn}}(\nu) \quad (2)$$

where $T_{\text{ff}}(\nu)$ and $T_{\text{syn}}(\nu)$ are the free-free and synchrotron emission contributions. By exploiting the information on the frequency dependence of each component, we have:

$$T_{\text{gal}}(\nu_1) = \left(\frac{\nu_1}{\nu_2}\right)^{\alpha_{\text{gal}}} T_{\text{gal}}(\nu_2) \quad (3)$$

$$T_{\text{ff}}(\nu_1) = \left(\frac{\nu_1}{\nu_2}\right)^{\alpha_{\text{ff}}} T_{\text{ff}}(\nu_2) \quad (4)$$

$$T_{\text{syn}}(\nu_1) = \left(\frac{\nu_1}{\nu_2}\right)^{\alpha_{\text{syn}}} T_{\text{syn}}(\nu_2) \quad (5)$$

In these expressions, α_{gal} , α_{ff} and α_{syn} are, respectively, the Galactic, free-free and synchrotron spectral indices. The validity of Eq. (2) together with Eqs. (3) to (5) lies in the fact that, although the sum of two power-laws is not a power-law, it can always be fitted with a power-law when only two frequencies are considered. Therefore, by combining Eqs. (3) through (5), it is possible to derive the fraction of thermal emission at each frequency. With some algebra, we obtain:

$$f_{\text{th},\nu_1} = \frac{1 - \left(\frac{\nu_2}{\nu_1}\right)^{\alpha_{\text{gal}} - \alpha_{\text{syn}}}}{1 - \left(\frac{\nu_2}{\nu_1}\right)^{\alpha_{\text{ff}} - \alpha_{\text{syn}}}} \quad (6)$$

We have set $\alpha_{\text{ff}} = -2.1$, while for α_{syn} we built a map of spectral indices as described in the following section. α_{gal} is computed by fitting the values of $T_{\text{gal}}(\nu)$ with ν respectively = 1.4, 2.7 and 5 GHz.

4.1 The synchrotron spectral index map

One of the major problems in performing a careful separation between the free-free and the synchrotron emission is the spatial variation of the synchrotron spectral index. In order to take this variation into account, we use the spectral index map obtained by Giardino et al. (2002). This map is constructed by combining data at 408 MHz, 1.4 and 2.3 GHz and has been convolved to a final resolution of 10° in order to remove the striation due to the scan-to-scan baseline errors in the input data. The initial maps have also been median filtered with a box of kernel of 9×9 pixels (given a pixel size of $\sim 13'$) to suppress the point source signal.

As discussed in Sect. 3, the Giardino et al. map is not really a full-sky synchrotron spectral index template. However, for latitudes above $3-4^\circ$, it can be regarded as a very good approximation to that. Below these latitudes, given the difficulty in obtaining an independent estimate of the free-free emission, it is not possible to have direct information on the synchrotron. At the same time, we do not expect a significant gradient in the synchrotron spectral index distribution within a few degrees from the plane. For this reason, we built a template of spectral indices for the selected region of the sky in the following way: we assume a spectral index between $b = -1.5^\circ$ to $+1.5^\circ$ similar to that between $|b| = 4^\circ$ to 5.5° for our selected region $l = 20^\circ$ to 30° . The spectral index between $|b| = 4^\circ$ to 5.5° is that given by Giardino et al. The average spectral index is $\alpha_{\text{syn}} = -2.73 \pm 0.02$. This is somewhat steeper than the typical spectral index of supernova remnants (SRNs), $\alpha_{\text{syn}} \sim -2.5$ (Green 2004), which contribute significantly to the synchrotron emission on the plane. However, we note that $\sim 10\%$ of the cataloged SNRs lie between $|b| = 4^\circ$ to 10° (Green 2004) so that their effect is only partly neglected by our analysis. At the same time, a real steepening of the spectral index is expected above $\sim 1 \text{ kpc}$ from the plane (Lisenfeld & Völk 2000). For a SNR at $D = 10 \text{ kpc}$, we are still within this range at $|b| = 5.5^\circ$. Given these combined effects, our approach appears as a viable approximation of the actual distribution of spectral indices.

Before illustrating the results of the application of Eq. (6), we discuss the validity of Eq. (4) with the assumption $\alpha_{\text{ff}} = -2.1$ over the range 1.4 GHz – 5 GHz.

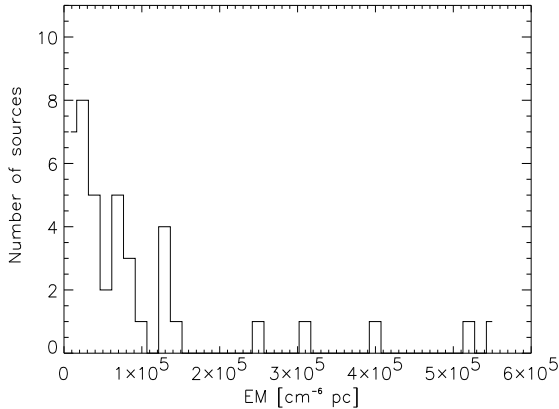


Figure 4. Emission measure distribution for 41 cataloged HII regions lying in the range $20^\circ < l < 30^\circ$, $-1.5^\circ < b < +1.5^\circ$. Data are from Downes et al. (1980) and Reifenstein et al. (1970).

4.2 The optical thickness regime for free-free emission in the range 1.4 GHz - 5 GHz

An important point of the analysis is the assessment of the emitting conditions of the ionized gas in the frequency range we are considering and, in particular, at 1.4 GHz. The expression for the optical thickness τ_ν^{ff} of thermal bremsstrahlung in the Altenhoff et al. (1960) approximation is, in CGS units:

$$\tau_\nu^{\text{ff}} \simeq 0.08235 T_e^{-1.35} \nu_{\text{GHz}}^{-2.1} (\text{EM}/\text{cm}^{-6} \text{ pc}). \quad (7)$$

If we assume the typical value $T_e \simeq 8000$ K which is common to both the diffuse ionized gas and HII regions, we see clearly that τ_ν^{ff} is proportional to the emission measure (EM). The EM is known to vary widely according to the form of ionized gas we are considering, i.e. diffuse gas or discrete, compact sources. For the diffuse gas, we use the reference value reported by Reynolds (1983) of $\text{EM} \simeq 9 - 23 \text{ cm}^{-6} \text{ pc}$. For this, at 1.4 GHz we obtain from Eq. (7) $\tau_\nu^{\text{ff}} \sim 1.9 \times 10^{-6} - 5. \times 10^{-6}$ and the optical thin regime applies. Alternatively, if we assume all the 5 GHz emission on the Galactic ridge to be free-free emission, then the upper limit to $T_{\text{b,ff}}$ is ≤ 15 K, i.e. $\tau < 2 \times 10^{-3}$ for $T_e = 8000$ K. As for HII regions, of the 102 compact sources lying in our selected coordinate range (see Sect. 5), 41 have an available estimate of the emission measure. The distribution of these values is shown in Fig. 4. Most of the sources are characterized by an emission measure $\text{EM} \sim 10^4$ to $10^5 \text{ cm}^{-6} \text{ pc}$ and only 20 percent have higher values, $> 10^5 \text{ cm}^{-6} \text{ pc}$. In the EM range $10^5 - 10^6 \text{ cm}^{-6} \text{ pc}$, τ_ν^{ff} varies in the range $\sim 0.02 - 0.2$ at 1.4 GHz. Again, since $\tau_\nu^{\text{ff}} < 1$, the assumption $\alpha_{\text{ff}} = -2.1$ is correct. Eq. (7) indicates that, at 1.4 GHz, τ_ν^{ff} is bigger than unity for values of the emission measure $\geq 5 \times 10^6 \text{ cm}^{-6} \text{ pc}$. These values of EM tend to characterize mainly UCHII whose flux density at these frequencies is rather faint. In summary, our adopted free-free emission spectral index appears to be correct over the frequency range 1.4 GHz - 5 GHz and the error introduced in the analysis by neglecting the presence of UCHII in our region of the sky is small.

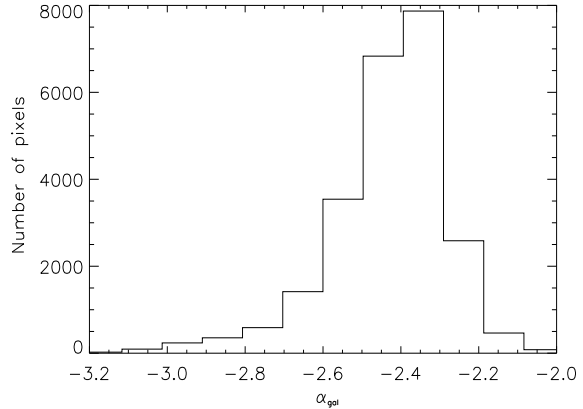


Figure 5. Galactic spectral index distribution between 1.4 GHz and 5 GHz. The mean value is $\overline{\alpha_{\text{gal}}} = -2.4 \pm 0.15$.

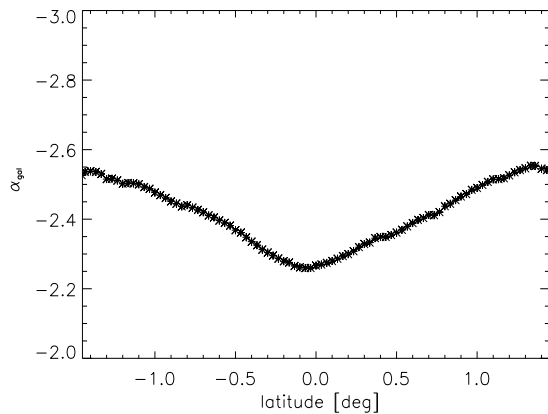


Figure 6. The spectral index variation with latitude of the total Galactic emission. The points are averages over longitudes in the range $20^\circ < l < 30^\circ$.

4.3 The Galactic spectral indices and the component separation

Before we can make the separation between free-free and synchrotron emission using the formalism of Eqs. (3) to (6), we compute, for each pixel in the selected coordinate range, the average spectral index, α_{gal} , in the frequency range 1.4, 2.7 and 5 GHz. The distribution of α_{gal} between 1.4 and 5 GHz for the selected area is shown in Fig. 5. The average value is $\overline{\alpha_{\text{gal}}} = -2.4 \pm 0.15$. The latitude variation in α_{gal} is shown in Fig. 6: there is a marked flattening of the spectral index on the Galactic plane towards the free-free emission value of -2.1 (with a maximum value of -2.25) demonstrating the dominance of free-free emission there. At a Galactic latitude of $b \sim 1^\circ$ however the synchrotron fraction is significantly larger with a value of $\alpha_{\text{gal}} \sim -2.5$.

By applying Eq. (6), we can compute the fraction of thermal emission at 1.4 GHz and 5 GHz. The variation of $f_{\text{th1.4GHz}}$ and f_{th5GHz} with latitude is shown in Fig. 7. The thermal fraction of the total emission clearly increases on moving towards the plane reaching a maximum value of 82% at $b = 0^\circ$ at 5 GHz; the corresponding value at 1.4 GHz is

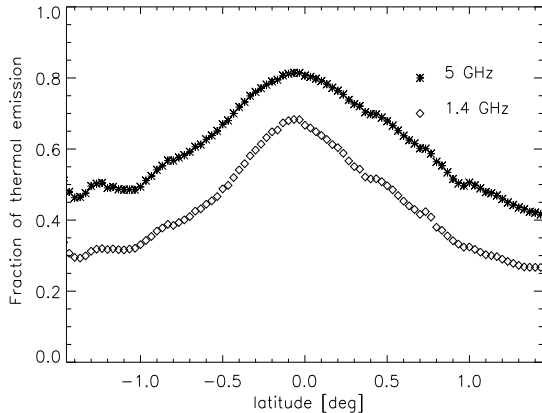


Figure 7. Fractions of thermal emission at 5 GHz (upper curve) and 1.4 GHz (bottom curve).

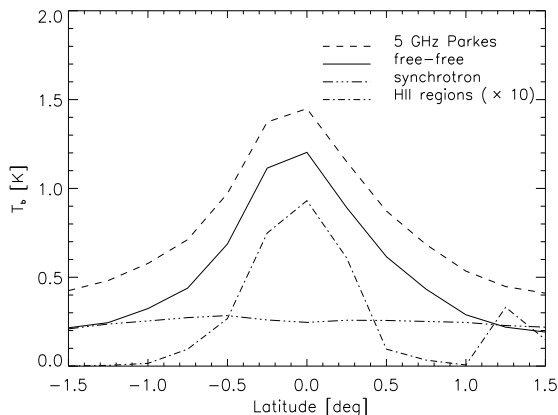


Figure 8. Latitude dependence of the total emission (dashed line), and of the free-free (solid line), synchrotron (double dotted-dashed line) and HII regions (dotted-dashed line) components for the 5 GHz Parkes survey. The free-free emission contribution is dominant within $\sim 1^\circ$ from the Galactic plane. At higher latitudes, the synchrotron fraction increases significantly with respect to the thermal component. Here, the HII regions profile has been multiplied by a factor 10.

68%. Hirabayashi (1974) has carried out 4.2 and 15.5 GHz measurements with $10'$ resolution of 9 points on the Galactic equator. Two of his points (denoted, in his work, as points A and B) fall in the region analyzed in this paper. At 15.5 GHz the free-free emission dominates, the synchrotron contribution being at the $\simeq 10\%$ level for $b \simeq 0^\circ$. Our approach yields $T_{\text{ff}}(15\text{GHz}) \simeq 0.103$ K for point A and $T_{\text{ff}}(15\text{GHz}) \simeq 0.091$ K for point B, in good agreement (being the difference of order of 30%) with the measurements by Hirabayashi (1974), corrected for our estimated synchrotron contribution.

5 THE FREE-FREE EMISSION COMPONENT AND THE CONTRIBUTION FROM HII REGIONS

We now proceed to separate the free-free emission component in the selected area $20^\circ < l < 30^\circ$, $-1.5^\circ < b < 1.5^\circ$. Using Eqs. (3) to (5) pixel by pixel, the fraction of thermal emission at 5 GHz can be estimated. The latitude number distribution is derived by averaging over longitude strips of the same size as the pixel side ($2'$). The distributions of free-free and synchrotron emissions are shown in Fig. 8. A simple gaussian fit to the free-free emission distribution at $|b| < 1.2^\circ$ gives a FWHM of $\sim 1.4^\circ$. The actual distribution is more complex, suggesting a narrow component on the Galactic plane.

A study of HII regions in the area throws light on the situation. There are 102 compact HII regions in the Paladini et al. (2003) catalog and 175 ultracompact HII regions in the Givon et al. (2004) catalog lying in the selected area. Their latitude distribution is well-fitted by a gaussian of FWHM = 0.8° . Clearly the free-free emission latitude distribution could be fitted with a narrow (FWHM = 0.8°) component comprising $\sim 80\%$ of the peak brightness temperature. The next question is how much of this emission is contributed by the ~ 300 cataloged HII regions. Fig. 9 shows the space distribution of the HII regions in the form of a brightness temperature map at 5 GHz made at $9.4'$ resolution. The contribution of the cataloged HII regions to the total free-free emission distribution, averaged over the range $20^\circ < l < 30^\circ$, is plotted in Fig. 8. By summing up the emission over the pixels for, respectively, the simulated HII-regions map and the derived free-free map, we can estimate the contribution of cataloged discrete sources to the total emission budget. The result is:

$$\frac{\sum_{j=1}^N T_{b\text{HII}_j}}{T_{b\text{ff}}} \simeq 9.2\%, \quad (8)$$

where $N = 277$, $T_{b\text{HII}_j}$ is the brightness temperature of the j -th HII region and $T_{b\text{ff}}$ is the brightness temperature of the free-free emission component at 5 GHz. Of this $\sim 9\%$ contribution to the total emission, $\sim 8\%$ is due to compact HII regions and only $\sim 1\%$ is given by ultracompact HII regions. It is important to note that the Paladini et al. catalog is confusion limited at rather bright flux densities (~ 7 Jy at 2.7 GHz), so that the total contribution of HII regions may be substantially higher.

6 CONCLUSIONS

We have presented the results of an analysis of the diffuse gas component in the thin layer of warm ionized gas. The analysis, performed in the coordinate range $20^\circ < l < 30^\circ$, $-1.5^\circ < b < +1.5^\circ$, has made use of radio continuum data at three different frequencies, namely 1.4 GHz, 2.7 GHz and 5 GHz. A decomposition of the total radio emission into free-free and synchrotron radiation has been carried out by exploiting the spectral dependence of each component. We present evidence that, on a $9.4'$ angular scale, the free-free emission fraction is contributed by both diffuse gas and discrete HII regions. In fact, a comparison of the latitude extension of the total free-free emission distribution with the

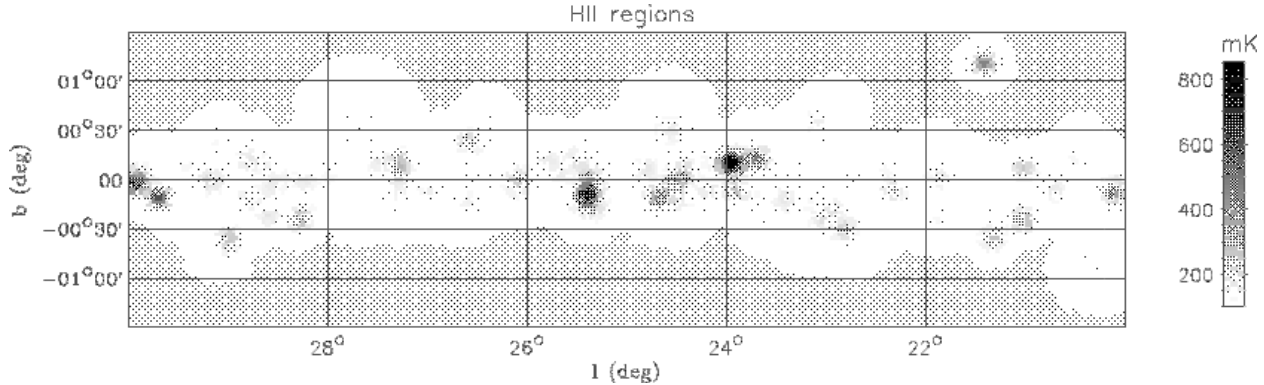


Figure 9. 5 GHz simulated map for 277 compact and ultracompact HII regions at a resolution of 9.4 arcmin. Flux densities and angular sizes are taken from Paladini et al. (2003). The colour scale is logarithmic.

latitude distribution of cataloged compact and ultracompact HII regions lying in the selected coordinate range indicates the presence of a dominant diffuse component at 5 GHz. Cataloged HII regions contribute only $\sim 9\%$ of the total emission budget. Although this is only a lower limit since the catalogs are confusion limited at rather bright fluxes, it is likely that a large fraction of the the remaining emission is accounted for by diffuse gas.

The errors in deriving the latitude distribution in our selected longitude range are mainly due to the uncertainty of the synchrotron spectral index which was adopted from the Giardino et al. 10 deg resolution spectral index map. Further progress will require more frequency data at $\sim 10'$ resolution such as will become available from the International Galactic plane Survey. A 2-D map of free-free (and synchrotron) emission on the Galactic plane should then become a possibility. At the same time, we point out that the correlation among neighbouring pixels does not undermine our results: despite the fact that the oversampling and convolution which have been performed on the original data sets introduce a level of correlation of order of 1%, given that all the operations involved are linear (e.g. averages in longitude), this effect can be neglected.

A complementary approach to obtaining the free-free emission distribution is to use radio recombination lines (RRLs) which, unlike $H\alpha$ emission, are unaffected by dust absorption and are not confused by synchrotron emission. The HIPASS (Stavely-Smith et al. 1996) and HIJASS (Boyce et al. 2001) surveys are now become available. However, an electron temperature is required to convert RRL line integrals to free-free brightness; the free-free emission distribution derived in the present paper can achieve this.

Further ancillary data relating to the electron distribution in the Galaxy come from several radio studies, including Dispersion Measurements of pulsars and Faraday Rotation measurements of pulsars and extragalactic sources. A recent promising initiative has been the use of Faraday Rotation of the diffuse Galactic synchrotron emission to map the Faraday screen as a function of depth (i.e. frequency) (Duncan et al. 1997; Uyaniker et al. 1998, 1999; Gaensler et al. 2001; Uyaniker et al. 2003). Such an approach gives information about the electron and magnetic field distribution.

ACKNOWLEDGMENTS

The authors thank the referee for helpful comments. They thank Giovanna Giardino for providing the processed version of the 408 MHz and 2.3 GHz maps, as well as for useful discussions. They also warmly thank Clive Dickinson for interesting comments and for making available the IDL routine which allows the conversion of the $H\alpha$ intensity into free-free emission. Finally, RP thanks Jean-Philippe Bernard for help in preparing the figures.

REFERENCES

- Altenhoff, W., Mezger, P. G., Wendker, H., Westerhout, G., 1960, Veröff Sternwarte Bonn
- Boyce, P. J., et al., ApJL, 560, 127
- Broadbent, A., Haslam, C. G. T. & Osborne, J. L., 1989, MNRAS, 237, 381
- Dickinson, C., Davies, R. D. & Davis, R. J., 2003, MNRAS, 341, 369
- Domgörgen, H. & Mathis, J. S., 1994, ApJ, 428, 647
- Duncan, A. R., Haynes, R. F., Jones, K. L., et al., 1997, MNRAS, 291, 279
- Fixsen, D. J., Cheng, E. S., Gales, J. M., Mather, J. C., Shafer, R. A., Wright, E. L., 1996, ApJ, 473, 576
- Gaensler, B. M., Dickey, J. M., McClure-Griffiths, N. M., et al., 2001, ApJ, 549, 959
- Giardino, G., Banday, A. J., Gorski, K. M., Bennett, K., Jonas, J. L. and Tauber, J., A&A, 2002, 387, 82
- Giveon, U., Becker, R. H., Helfand, D. J. et al., astro-ph/0410052
- Green, D. A., 2004, Bulletin of the Astronomical Society of India, 32, 335
- Haslam, C. G. T., Salter, C. J., Stoffel, H. & Wilson, W., 1982, A&AS, 47, 1
- Haynes, R. F., Caswell, J. L., Simons, L. W. J., 1978, Aust. J. Phys. Astrophys. Suppl., 45, 1
- Hirabayashi, H., 1974, Publ. Astron. Soc. Japan, 26, 263
- Howell, T. F. & Shakeshaft, J. R., 1967, Nature, 216, 753
- Jonas, J. L., Baart, E. E. & Nicolson, G. D., 1998, MNRAS, 297, 977
- Lisenfeld, U. & Völk, H. J., 2000, A&A, 354, 423
- Miller, W. W. & Cox, D. P., 1993, ApJ, 417, 579
- Paladini, R., Burigana, C., Davies, R., et al., 2003, A&A, 397, 213
- Paladini, R., Davies, R., DeZotti, G., 2003, MNRAS, 347, 327
- Platania, P., Burigana, C., Maino, D. et al., 2003, A&A, 410, 847
- Reich, W., 1982, A&AS, 48, 219

- Reich, P. & Reich, W., 1986, A&AS, 63, 205
Reich, P. & Reich, W., 1988, A&AS, 74, 7
Reich, P., Reich, W., Fürst, E., 1990, A&A, 83, 539
Reich, W., Fürst, E., Reich, P., Reif, K., 1990, A&AS, 85, 633
Reif, K., Reich, W., Steffen, P. Muller, P., Weiland, H., 1987,
Mitt. Astron. Ges, 70, 419
Reynolds, R. J., 1983, ApJ, 268, 698
Schlegel, D. J., Finkbeiner, D. P. & Davis, M., 1998, ApJ, 500,
525
Staveley-Smith, L., et al., PASA, 13, 243
Taylor, J. H. & Cordes, J. M., 1993, ApJ, 411, 674
Uyaniker, B., Fürst, E., Reich, W., et al., 1998, A&AS, 132, 401
Uyaniker, B., Fürst, E., Reich, W., et al., 1999, A&AS, 138, 31
Uyaniker, B., Landecker, T. L., Gray, A. D., et al., 2003, ApJ,
585, 785